PROCEEDINGS OF SPIE

SPIEDigitalLibrary.org/conference-proceedings-of-spie

Absolute surface metrology of x-ray telescope mirrors through axial shift mapping

Hayden Wisniewski, Ralf Heilmann, Mark Schattenburg, Brandon Chalifoux

Hayden J. Wisniewski, Ralf K. Heilmann, Mark L. Schattenburg, Brandon D. Chalifoux, "Absolute surface metrology of x-ray telescope mirrors through axial shift mapping," Proc. SPIE 12679, Optics for EUV, X-Ray, and Gamma-Ray Astronomy XI, 126790Q (5 October 2023); doi: 10.1117/12.2677596

SPIE.

Event: SPIE Optical Engineering + Applications, 2023, San Diego, California, United States

Absolute surface metrology of X-ray telescope mirrors through axial shift mapping

Hayden J. Wisniewski[a], Ralf K. Heilmann[b], Mark L. Schattenburg[b], and Brandon D. Chalifoux[a,*]

[a]James C. Wyant College of Optical Sciences, The University of Arizona, 1630 E University Blvd. Tucson, Az USA 85721

[b]Space Nanotechnology Laboratory, MIT Kavli Institute for Astrophysics and Space Research, Massachusetts Institute of Technology, 77 Massachusetts Avenue, Cambridge, MA USA 02139

ABSTRACT

The next generation of X-ray telescopes will require mirror segments to be characterized to a surface uncertainty of 5 nm RMS or better. We present axial shift mapping, a Fizeau interferometry method to characterized near-cylindrical null correctors and surfaces. We extend our previously tested technique to cylindrical optics of similar dimensions to X-ray telescope mirrors. We report on progress towards full surface extraction of a cylindrical optic using axial shift mapping.

Keywords: X-ray mirror metrology, absolute metrology, interferometric metrology methods, computer generated hologram, optical metrology, X-ray telescope

1. INTRODUCTION

Fizeau interferometry is a foundational method for measuring the surface figure of optical surfaces with high precision. Flat and spherical reference surfaces (transmission flats and transmission spheres, respectively) are commonly characterized to $\lambda/20$ peak to valley (PV) which can be assumed as ground truth for most measurements.[1] A challenge when moving to non-rotationally symmetric surfaces is accurately generating the test wavefront, which must approximately match the surface under test (SUT). For cylindrical optics, this requires a specially designed refractive transmission cylinder or computer generated hologram (CGH) that resides in the optical cavity.[2–4] These null optics in the non-common path portion of the interferometer add uncertainty to surface measurements. Self-referencing tests allow the extraction of the true SUT surface figure without direct influence from the uncertainty of the null optics or reference surface.[5–8] Here we present axial shift mapping (ASM), a self-referencing surface metrology technique aimed at extracting the axial surface figure of a cylindrical SUT from a set of Fizeau measurements without the effect of the null optics.

X-ray telescope mirrors are off-axis parabaloids and hyperboloids that reflect X-rays at glancing incidence with a Wolter Type I prescription,[9] a rendering of which can be seen in Figure 1a. The next generation of high-resolution X-ray telescopes are aiming for sub-arcsecond angular resolution (half-power diameter), which requires an axial figure error around 5 nm RMS. Beyond this, X-ray telescopes and interferometers with micro-arcsecond resolution are being designed[10–12] that would require axial figure of $\lambda/200$ RMS (at $\lambda = 633$ nm) for the near 1.2 keV (= 1 nm) X-ray band and $\lambda/1000$ RMS for the near 6 keV (= 0.2 nm) X-ray band.[12] To achieve this with Fizeau interferometry, it will be necessary to either characterize the null optics to below these levels or implement a self-referencing method that extracts the surface under test (SUT) without influence from the reference surface and null optics.

While X-rays reflect off the mirrors at glancing incidence (i.e., at small angles to the y-axis in Figure 1b), the mirrors are more easily measured near normal incidence (i.e., along the z-axis), making the mirrors nearly cylindrical. Axial figure error degrades imaging performance far more than figure errors along the sagittal direction.[13] The nominal figure is typically dominated by a quadratic figure term that must be tightly controlled for all telescope mirrors to have a common focal length.[9]

*bchal@arizona.edu

Optics for EUV, X-Ray, and Gamma-Ray Astronomy XI, edited by Stephen L. O'Dell, Jessica A. Gaskin, Giovanni Pareschi, Daniele Spiga, Proc. of SPIE Vol. 12679, 126790Q · © 2023 SPIE · 0277-786X · doi: 10.1117/12.2677596

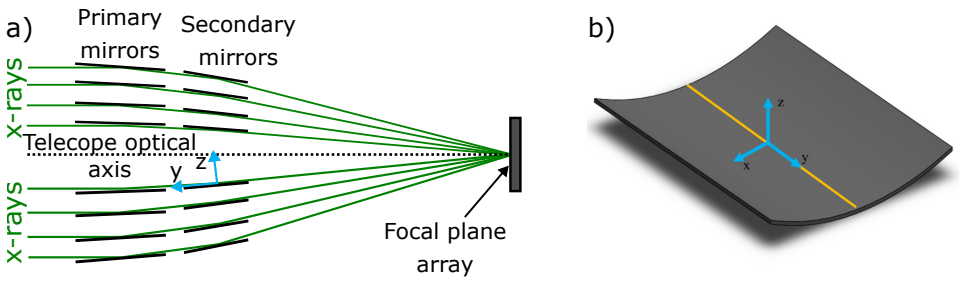

Figure 1. ASM may be applied to improve X-ray telescope mirror metrology. *a*) A Wolter type 1 X-ray telescope. The primary mirror is composed of nested off-axis parabolas and the secondary mirror is composed of nested off-axis hyperbolas. A ring can be separated into many segments that are then assembled and aligned. *b*) A single X-ray telescope mirror segment. The axial profile, traced for one azimuthal position as the orange line along the y direction, is crucial for system performance.

ASM is a lateral shear type self-referencing method, where we translate the SUT between measurements along the axial profile to extract the axial profile of the SUT without the influence due to the reference surface or null optics, and vice versa. In lateral shear self-referencing tests, rigid body errors during shifting introduces a quadratic ambiguity due to a necessary integration operation.[14,15] For cylindrical surfaces, two rigid body error rotations affect the quadratic term along the axial profile, namely pitch (rotations around x) and roll (rotations around z). Other rigid body error motions do not affect axial figure measurement. We place two known artifact mirrors (KAMs) in the field of view of the interferometer to measure both pitch and roll and break the quadratic ambiguity, expanding lateral shear type measurements to include sagittally-curved surfaces. We show the mathematical basis for ASM, discuss the experimental method, and show results for the full surface extraction of a cylinder along the axial profile.

2. AXIAL SHIFT MAPPING THEORY

2.1 Shift mapping

A lateral shearing technique for measuring optical flats was introduced by Bloemhof in 2010[6] which involves taking three measurements, one at a nominal position and then two measurements shifted by one pixel in orthogonal lateral directions. While this is the first instance to our knowledge where this method was described for Fizeau interferometry, shearing metrology has its roots in multi-sensor interferometric probes.[14,15] This technique was expanded upon to show that the system could be shifted by more than a single pixel.[16] The downside of increasing the pixels per shift is that the extracted surface becomes blind to spatial frequencies at the pixel per shift spatial wavelength, and the edges have higher uncertainty.[15]

For X-ray telescope mirrors that reflect at glancing incidence, the surface figure along the axial direction is crucial for system performance. We previously demonstrated our ability to extract single line traces of flat mirrors.[17,18] We now show how we expand this self referencing metrology technique to the axial direction for cylindrical systems. Unlike the method presented by Bloemhof, this will only require a shift along the axial direction of the mirror. The full surface of the cylinder will be extracted, but due to only shifting axially, radial traces may include influence due to the reference surface. To extract a true 2D topography requires a rotation around the center of curvature of the mirror and higher computation power to extract the surfaces, which is beyond the scope of the current experiment.

A Fizeau measurement of a cylindrical surface can be written as

$$M_0(\phi, y) = T(\phi, y) - R(\phi, y), \tag{1}$$

where T is the height in the surface map of the SUT, and R is the height produced by the reference surface and null optics (more precisely, half the OPD) at the cylindrical coordinates (ϕ, y), with the orgin at the center of curvature of the mirror. If we then shift the SUT by a distance of Δy, equation 1 becomes

$$M_1(\phi, y) = T(\phi, y + \Delta y) - R(\phi, y), \tag{2}$$

where Δy is along the axial direction of the mirror and the subscript 1 indicates that it has shifted $1 \times \Delta y$ from the nominal position (Figure 2). In the measurements, contributions in the interferogram due to the SUT shift while contributions due to the reference surface are static.

We take a difference between the shifted map and the nominal map and obtain

$$M_1(\phi, y) - M_0(\phi, y) = T(\phi, y + \Delta y) - T(\phi, y), \tag{3}$$

where contributions due to the reference surface have been eliminated. This represents the slope information of the SUT. To obtain the surface height information, we integrate this extracted surface slope information, or equivalently, solve a matrix equation.

While direct integration will provide the desired information, we want to retrieve the information with as little measurement noise as possible. We use a Moore-Penrose pseudo inverse matrix,[19] by setting up the matrix system

$$\mathbf{K}\vec{z} = \vec{m}, \tag{4}$$

where $\vec{z}$ is a vector containing the true surface points, $\vec{m}$ is a vector containing measurements, and $\mathbf{K}$ is a matrix that relates them through equation 3. If we are describing a single line along a surface, we construct $\vec{z}$ as

$$\vec{z} = \begin{bmatrix} R_1 & \dots & R_I & T_1 & \dots & T_I \end{bmatrix}^{\mathbf{T}}, \tag{5}$$

where R_i and T_i are the actual value of the reference surface and SUT respectively at pixel i, up to the max number of pixels I. While a minimum of two measurements are required, because this is a least mean squares method, we can readily solve an over-constrained system of equations, performing the extraction with more than the nominal and shifted measurement. If we take J measurements, we construct $\vec{m}$ as

$$\vec{m} = \begin{bmatrix} m_{1,0} & \dots & m_{I,0} & m_{1,1} & \dots & m_{I,1} & \dots & m_{I,J} \end{bmatrix}^{\mathbf{T}}, \tag{6}$$

where the first subscript indicates pixel location and the second indicates shift number. Each measurement is concatenated to the end of the previous measurement. We build the $\mathbf{K}$ matrix according to equation 1.

We build the $\mathbf{K}$ matrix and our measurements will give us the values to form $\vec{m}$. We perform the pseudo-inverse

$$\vec{z} = (\mathbf{K}^{\mathbf{T}}\mathbf{K})^{-1}\mathbf{K}^{\mathbf{T}}\vec{m}, \tag{7}$$

and the extracted $\vec{z}$ will contain the actual values of the reference surface and the SUT. Since the pseudo-inverse is a least mean squares method, the more we shift the SUT, the more information is used to extract the surfaces. The number of measurements taken must balance the benefit of more information being used to inform the final surfaces, with physical effects, such as data loss at the edges due to shifting, and changing environmental conditions that cause deformation and measurement drift. This formulation is for extracting a single line of data. If we want to extract a surface composed of singular lines of data, then we horizontally concatenate their information to $\vec{m}$ and concatenate columns to $\vec{z}$ to hold the extracted lines of information.

2.2 Quadratic ambiguity

During the axial shift, rigid body errors will be introduced. When taking the difference as described by equation 3, a rigid body error of a pitch (rotation about x in figure 1) of the SUT will create a linearly-varying slope measurement. When this linear term is integrated, it presents itself as a quadratic term in the height information. This can mask a true quadratic term in the surface or reference.[14] Here we mathematically describe how this quadratic ambiguity, as named by Huang,[20] arises and how we break the ambiguity with a known artifact mirror (KAM) in the field of view of the interferometer.

The quadratic ambiguity arises from an inadvertent rotation of the SUT (T) between shifts, the effect of which is indistinguishable from quadratic errors in either the SUT or reference (R). This is readily illustrated with a simple example of a SUT and reference surface each represented as purely quadratic surfaces,

$$\begin{aligned} T_0 &= \kappa_T y^2 \\ R_0 &= \kappa_R y^2, \end{aligned} \tag{8}$$

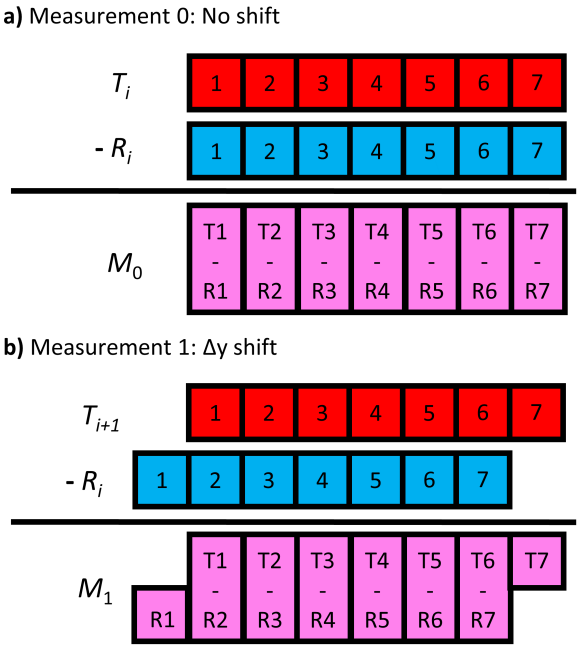

Figure 2. Measurement 0 is taken at the nominal position. The SUT is then shifted along the desired direction by Δy giving measurement 1. The difference between these measurements gives the slope space information of the SUT. This information is integrated to return the surface height of the SUT, which is then used to determine the reference surface.

where κ is the curvature of the surface. The subscript zero indicates that this is the measurement at the nominal location.

If we shift the test surface laterally by a value of Δy, the surface becomes

$$T_1 = \kappa_T (y + \Delta y)^2 + \theta y, \tag{9}$$

where θ is the unknown tilt due to rigid body errors of the stage motion. The measurements are the addition of the reference surface with the test surface,

$$M_0 = \kappa_R y^2 + \kappa_T y^2, \tag{10}$$

and

$$M_1 = \kappa_R y^2 + \kappa_T (y + \Delta y)^2 + \theta y. \tag{11}$$

The difference between these measurements can lead to

$$\frac{\Delta M}{\Delta y} = \left(2\kappa_T + \frac{\theta}{\Delta y}\right) y + \kappa_T \Delta y, \tag{12}$$

which shows that in addition to the $\kappa_T \Delta y$ term (rigid body tilt), we are left with an error in the curvature of $\theta/2\Delta y$ in slope space. Therefore, we must measure this tilt θ to accurately reconstruct the surface. In general, real surfaces contain terms of higher order than quadratic, which can also contribute to the quadratic ambiguity.

A KAM in the field of view of the interferometer modeled as,

$$K_0 = \kappa_K y^2, \tag{13}$$

is precharacterized to have a known κ_K. This means that it does not have the ambiguity as described by equation 12. This property is exploited to retrieve the rigid body error induced during shifting and break the quadratic ambiguity of the SUT.

2.3 2D quadratic ambiguity

The quadratic ambiguity in lateral shear methods is not contained to a single direction. For a cylindrical SUT, multiple rigid body errors can create a quadratic ambiguity. A model described by Robinson and Reardon states that the surface height error due to a rigid body error of a cylindrical surface, δW, can be described by[21]

$$\delta W = \overrightarrow{t} \cdot \hat{n} + \overrightarrow{\theta} \cdot (\overrightarrow{r} \times \hat{n}), \tag{14}$$

where $\overrightarrow{t}$ is a vector of the translation $\overrightarrow{t} = \begin{bmatrix} \epsilon_x & \epsilon_y & \epsilon_z \end{bmatrix}^T$, θ is a vector containing the rotations $\overrightarrow{\theta} = \begin{bmatrix} \theta_x & \theta_y & \theta_z \end{bmatrix}$, $\overrightarrow{r}$ is the position vector from the center of rotation to each surface location i,

$$\overrightarrow{r} = \begin{bmatrix} r_{x,1} & r_{x,2} \dots r_{x,N} \\ r_{y,2} & r_{y,2} \dots r_{y,N} \\ r_{z,3} & r_{z,2} \dots r_{z,N} \end{bmatrix}, \tag{15}$$

and $\hat{n}$ is the unit normal vector of the surface. θ_x corresponds to a pitch rotation of the mirror, which we demonstrated will induce a quadratic ambiguity. θ_z represents a roll rotation of the mirror, and according to equation 14, this will create an astigmatic height error, which is the equivalent of a linearly varying pitch across the surface. For a cylindrical surface, both a pitch and roll will create a quadratic ambiguity in the extracted surface. Therefore, both pitch and roll of the surface during shifting must be measured and subtracted to determine the quadratic term.

Two KAM mounted at an azimuthal position $\pm\phi_{\mathrm{K}}$ and tilted at angle $\pm\phi_{\mathrm{K}}$ can be mounted on either side of the SUT to mitigate the 2D quadratic ambiguity.If a local coordinate frame of (r, s, t) is defined in the center of each KAM with r along the mirror radial direction and t along the azimuthal direction, then every tilt measurement of the KAM will produce a measured rotation about t, θ_t. We relate this to a pitch, θ_x, and roll, θ_z, of the mirror through

$$\theta_x = \frac{\theta_{t,R} + \theta_{t,L}}{2\cos\phi_{\mathrm{K}}}, \tag{16}$$

and roll as

$$\theta_z = \frac{\theta_{t,R} - \theta_{t,L}}{2\sin\phi_{\mathrm{K}}}, \tag{17}$$

which gives rigid body errors in two dimensions.

3. EQUIPMENT AND METHODS

This section details the system used for extraction (Section 3.1), a detailed description of the CGH and mirror mounting scheme (Section 3.2), and the method for extracting the full surface (2D) of a cylindrical optic using ASM (Section 3.3). The coordinate frame as referenced by the paper can be seen in Figure 1.

3.1 System design

Aside from the SUT and CGH, ASM makes use of a Fizeau interferometer, an optical flat for a reference surface, a 6 degree of freedom (DOF) motion system for the SUT, a tip-tilt stage for the CGH, and KAMs. The Fizeau interferometer (Äpre Instruments Inc. S100) has a 2048×2048 pixel detector array. Each pixel is 50.8 μm square when projected into test space. The interferometer was equipped with a $\lambda/20$ PV transmission flat coated for high fringe visibility with highly reflective surfaces, which served as the reference surface. Each interferometer measurement consisted of 10 phase shifting cycles averaged together. The 6 DOF motion system is composed of multiple independent stages. Translational motion is handled by a separate Z stage (Aerotech AVS100) and XY stage (Aerotech ANT110). Rotational motion is provided through a tip/tilt/rotation stage (Newport 37) with motorized actuators (ThorLabs Z825B). The KAMs are Corning ultra-low expansion (ULE) flat mirrors (10 mm $\times$ 10 mm $\times$ 75 mm, coated with a multilayer film for high reflectivity at 633 nm wavelength). The KAMs were measured using a three-flat test, prior to each experiment, after mounting in their respective fixtures. An image of the experimental setup for the 2D extraction can be seen in Figure 3.

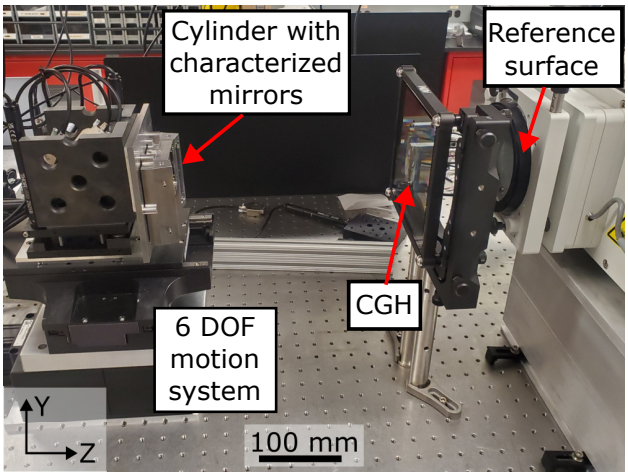

Figure 3. 2D extraction system including the interferometer with an optical flat as the reference surface, the CGH, and the cylinder SUT with the two side mirrors sitting on the 6 DOF stage system. We use the 6 DOF stage system to kinematically translate and rotate the SUT.

3.2 Computer Generated Hologram and mirror mounting geometry

Measuring a cylindrical mirror required a null optic that generates both a cylindrical wavefront and planar wavefronts for measuring KAM tilts, as well as a mounting method for the cylindrical SUT and two KAMs. A diagram of the setup for cylinder measurements can be seen in Figure 4. A CGH (produced by Arizona Optical Metrology, LLC.) was placed between the reference surface and the SUT, which was designed so the $m = 1$ diffraction order produced the desired wavefronts.

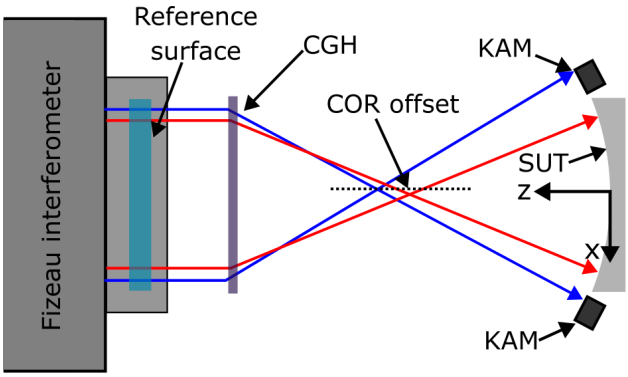

Figure 4. Diagram of the interferometer and CGH system including the KAMs. The KAMs are tilted at ϕ_K, and the planar wavefront for the KAMs come from the opposite side of the cylinder CGH and cross at the cylinder center of curvature. The center of rotation (COR) may be slightly offset due to a the choice to offset the KAMs. KAM tilts allow pitch and roll measurements through equations 16 and 17.

An image of the mirror mount is shown in Figure 5 and a photograph of the CGH can be seen in Figure 6. To mount the three mirrors, we designed steel capsules that would hold each mirror and mount to a common plate. The cylindrical mirror is mounted in the center, and a KAM is mounted on either side. The two KAMs are angled at $\phi_{\mathrm{K}} = \pm 13.9$ degrees, which allows measurement of the roll. We chose steel as the mounting material, to balance cost with CTE mismatch between the ULE and mount, compared to aluminium. The SUT is a 50.8 mm by 50.8 mm concave cylindrical mirror with a radius of curvature of $R = 138$ mm (Newport CSV300), which we coated with 100 nm electron beam evaporated platinum.

The CGH is a chrome amplitude grating on a fused silica substrate with a $< 0.1\%$ anti-reflection coating on the back surface. Centered on the CGH is a 50.8 mm by 50.8 mm grating that diffracts light into a cylindrical wavefront that focuses to a line at $f = 138$ mm away and then propagates and matches the $R = 138$ mm of

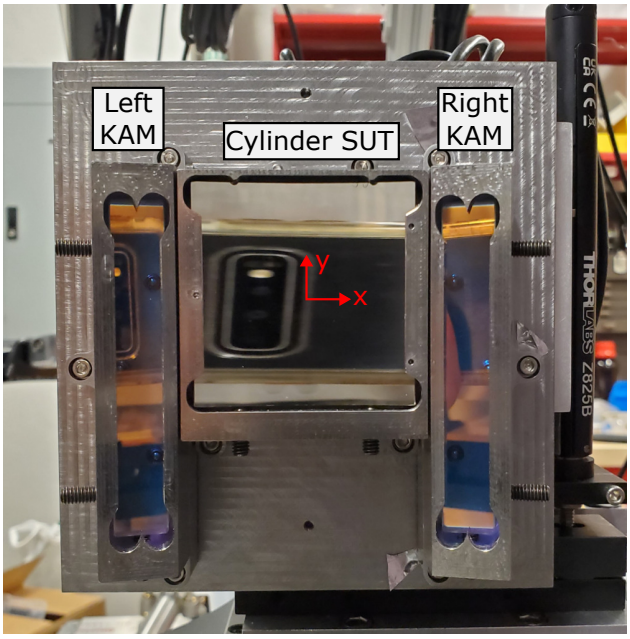

Figure 5. Photograph of the cylinder mirror with accompanying left and right side mirrors tilted at ±13.9 degrees. Mirrors were mounted in separate capsules to ease in in alignment.

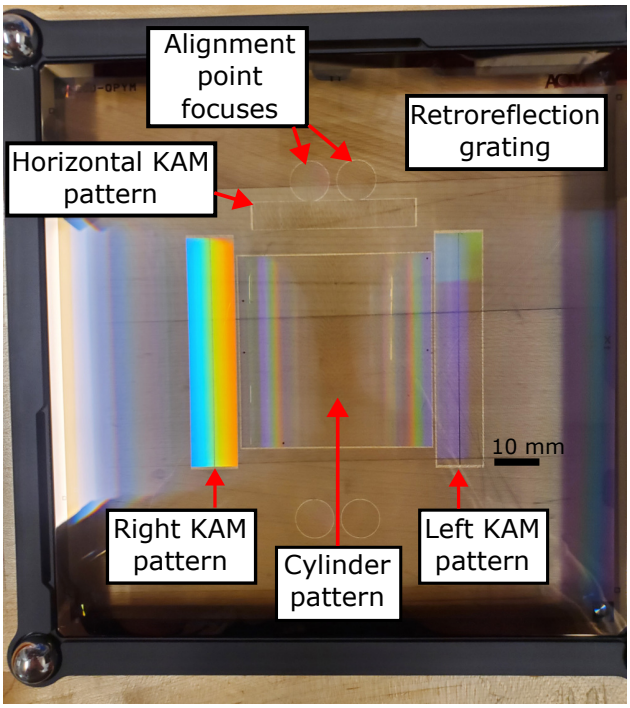

Figure 6. Photograph of the CGH that generates a cylindrical wavefront from the center for the SUT, planar wavefronts for KAMs, and alignment foci. The KAM patterns are labeled as for their corresponding mirror. The Horizontal KAM pattern is not used in this work. The CGH gives the flexibility of design required to incorporate KAMs into the system.

the SUT. On either side of the cylinder pattern is a 60 mm by 5 mm planar wavefront grating that generates a wavefront towards the KAM on the opposite side of the SUT. Four alignment point focuses diffract light to focus at the corner of the SUT for rough alignment. In the space between the written gratings is a retroreflection grating that aids in aligning the CGH to the interferometer at the desired angle. There is a horizontal KAM

pattern (along the x direction) that is used for angle measurements in radial extractions that is not used in the current work.

Each planar wavefront hologram has two different patterns. These extra patterns will produce null fringes on the KAMs when the system is shifted around the center of curvature by 0.72 mrad, which is used for radial 2D extraction. The KAMs can be nulled to either the interior or exterior pattern for the corresponding KAM. When an interior pattern is used for one KAM and an exterior pattern is used for the other KAM, an offset occurs between the measured center of rotation (COR) and axial line focus of the mirror (Figure 4). Our experimental set up generates a 1.75 mm COR offset when offset patterns are used. This can be compensated for by redefining the normal vectors of the surface in equation 14 with this new COR. When both interior or exterior KAM patterns are used, no COR offset occurs.

3.3 2D cylindrical mirror measurement

We applied ASM along the axial direction (y) of a cylindrical surface. Every axial trace of the reference surface and the SUT were extracted. The measurement parameters for the five measurement campaigns of 2D ASM are shown in Table 1

To mitigate any remaining retrace error and maintain the small angle assumption of equation 14, we implemented an active alignment system based on the information gathered from the KAMs to mitigate any negative effects due to large tilts during shifting. The active alignment is done in an iterative process using the 6 DOF stage system, which mechanically nulls the SUT using the information of pitch and roll as extracted through equation 16 and equation 17. The mechanical nulling is repeated until the pitch is below a preset angle tolerance. Once the measured pitch is below the angle tolerance, the remaining angle is mathematically nulled out though equation 14. Due to the active alignment procedure, the total time of measurement is variable with the extra measurements required to align the mirror. For a single set of 20 measurements, a typical measurement time was approximately 20 minutes.

Both the left and right KAM were measured after mounting, using a three flat test. Along the center line, the left KAM has surface figure of 259.5 nm RMS and a curvature of $\kappa_{K,L} = -8.04 \times 10^{-4}$ m^{-1}. The right KAM was determined to have a surface figure of 43.9 nm RMS of figure error with a curvature of $\kappa_{K,R} = -1.34 \times 10^{-4}$ m^{-1}. During the full set of measurements a peak to valley temperature difference was found to be 50 mK.

When a KAM has higher order surface terms, the quadratic ambiguity extraction requires these higher order terms to be included. However, we can use the measured profile of the KAM to determine the tilt θ_K than can be expected when we shift a KAM with no rigid body errors. For each measurement at shift distance j, we take the measured profile and shift it by j pixels. We subtract this shifted line from the measured profile at the original position. We add the slope of this difference measurement, θ_K, to our measured tilt angles $\theta_{t,R}$ and $\theta_{t,L}$ (equations 16 and 17) to minimize effects due to the KAM profile.

During analysis, Each measurement was read in and the remaining measured pitch and tilt were mathematically removed from each surface according to equation 14. The 20 measurements were stacked into one $\overrightarrow{m}$ that is L wide by $I \times J$ long, where L is the number of lines on our surface, I is the number of pixels, and J is the number of measurements. A $\mathbf{K}$ matrix of size $(IJ \times 2I)$ was constructed that corresponds to a single- or double-pixel shift for 20 measurements, depending on the measurement campaign. This $\mathbf{K}$ matrix was inverted using the pseudo-inverse and it was multiplied by $\overrightarrow{m}$ which calculated our $\overrightarrow{z}$. Since this method was only applied

Table 1. Measurement parameters for separate campaigns of 2D ASM on a cylindrical surface.

Campaign	Sets	Measurements per set	Pixels per shift	Angle Tolerance (μrad)	offset (mm)
1	10	20	1	1.5	1.75
2	10	20	1	1.5	1.75
3	7	20	1	1	1.75
4	10	20	2	1	1.75
5	10	20	2	1	0

along the axial direction, each axial trace is independent, and we subtract the mean and best fit line of each trace.

The CGH manufacturer's bottom up error analysis asserts that transmitted wavefront error (TWE) of the fused silica substrate is the dominant error term of the CGH. To compare ASM against another measurement technique, the TWE of the CGH was measured using spectrally controlled interferometry or SCI (Äpre Instruments SpectrÄ source), where we create interference between the two surfaces of the substrate. This measures the optical thickness variation of the substrate, $n\left(t\left(x,y\right)-\bar{t}\right)$ (where $n=1.457$ is the refractive index of fused silica at $\lambda=633\ nm$ and t is the thickness of the substrate), from which we calculate the associated TWE $=\left(t\left(x,y\right)-\bar{t}\right)\left(n-1\right)/n$.[22] We compare the SCI extracted TWE to the ASM measured reference surface to determine the reliability of our method.

The repeatability of ASM was determined through performing multiple ASM shifting procedures on the SUT. Five different measurement campaigns were preformed on the same SUT. The extracted SUT and reference surface of each campaign were then averaged to generate an averaged measured SUT and reference surface. The repeatability is reported as the difference between the five campaign average and the the current campaign.

4. RESULTS AND DISCUSSION

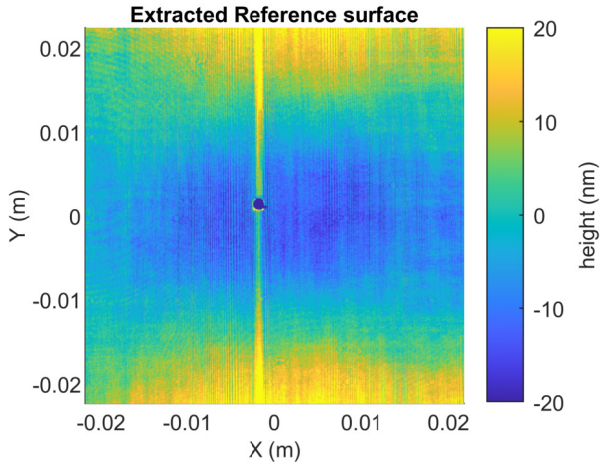

Figure 7. Reference surface averaged over 5 measurement campaigns of extraction. The average repeatability of the extracted reference surface is 4.4 nm RMS.

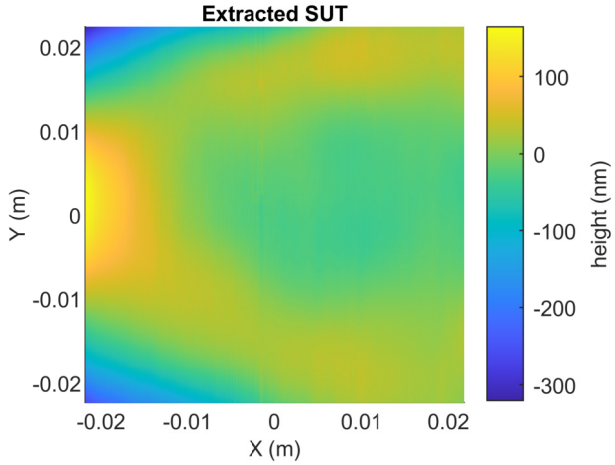

Figure 8. Test surface averaged over 5 measurement campaigns of extraction. The average repeatability of the extracted SUT is 4.4 nm RMS.

The five measurement campaigns of the cylindrical surface were carried out according to the parameters as defined in Table 1. The reference surface and SUT were extracted for each campaign through averaging the extracted surface from each set. The extracted reference surface and SUT as averaged over the five campaigns can be seen in Figure 7 and Figure 8 respectively. Comparing the surfaces of each campaign against the five campaign average, we calculated the repeatability for each campaign. The average repeatability extracting the reference surface and the SUT were both 4.4 nm RMS. Table 2 shows the repeatability of each measurement campaign. The system was less repeatable for a two pixel per shift measurements, the cause of which is an avenue for future work.

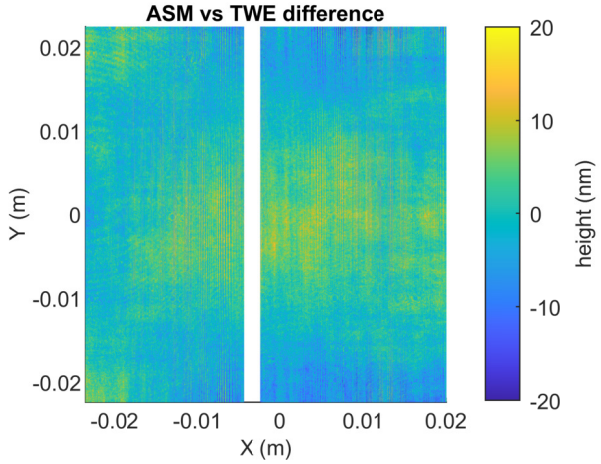

Figure 9. Difference between the TWE of the reference surface as extracted through ASM and as extracted through SCI. The average standard deviation of the difference between the two surfaces is 4.5 nm RMS.

A graph showing the comparison of the reference surface as extracted through ASM against the TWE as extracted by SCI can be seen in Figure 9. There is a column of missing data in the resulting figure, which is due to diffraction effects of the CGH. The results of these diffraction effects can be seen in the same column of data in Figure 7. This surface was generated for all five measurement campaigns and the standard deviation of this difference can be seen in Table 2. The average standard deviation of the difference between these two surfaces is 4.5 nm RMS. This confirms that the TWE is the dominant factor in the error of the CGH. The remaining error may be due to either ASM or the CGH, from sources such as retrace error, CGH pattern error, reference surface flatness, or inaccuracies introduced from ASM.

5. CONCLUSION

We presented ASM, a self referencing metrology technique for cylindrical surfaces that can be applied to acylindrical surfaces such as X-ray telescope mirrors. ASM extracts the axial profiles of the SUT and reference surface

Table 2. Measurement results with SUT and reference surface repeatability and extracted reference surface compared to a known method.

Campaign	SUT repeatability (nm RMS)	Reference repeatability (nm RMS)	Comparison (nm RMS)
1	2.7	2.7	4.3
2	1.9	2.7	3.8
3	2.7	2.9	4.5
4	5.2	4.6	5.1
5	9.6	9.2	4.7
Mean	4.4	4.4	4.5

through shifting the SUT between measurements. This shift induces an inherent quadratic ambiguity due to rigid body errors, and we demonstrated a method to break this quadratic ambiguity through the use of KAMs in the field of view of the interferometer.

We measured a cylindrical mirror using ASM. Measuring the cylindrical mirror over five measurement campaigns with varying parameters, we extracted the surfaces with a 4.4 nm RMS repeatability. When comparing the extracted reference surface with the independently measured TWE of the CGH substrate, which we expect to be the largest (but not only) error source of the CGH, we found an average difference of 4.5 nm RMS over the five campaigns. Our surface extraction of the reference surface confirmed that the transmitted wavefront error is the dominate source. Avenues of future work include: investigating error sources that could contribute to the measurement error, expanding ASM to axial and azimuthal surface profile extraction, and expanding to measure X-ray telescope mirrors. To our knowledge, this ASM the first 2D self-referencing method to measure cylindrical optics including the quadratic term that is so important for X-ray telescope mirrors.

ACKNOWLEDGMENTS

We would like to thank Will Zhang at NASA Goddard Space Flight Center, Heng Zuo at University of New Mexico, and Mallory Whallen at Massachusetts Institute of Technology for engaging in conversations during the projects lifetime. We would also like to thank Arizona Optical Metrology for their aid in designing the CGH. This work was funded by NASA grants 80NSSC20K0907 and 80NSSC22K1484.

REFERENCES

[1] Schulz, G. and Schwider, J., "Iv interferometric testing of smooth surfaces," in [*Progress in Optics*], Wolf, E., ed., **13**, 93–167, Elsevier (1976).

[2] Coyle, L. E., *Precision Alignment And Calibration Of Optical Systems Using Computer Generated Holograms*, PhD thesis, The University of Arizona. (2014).

[3] Burge, J. H., "Null test for null correctors: error analysis," in [*Proc. SPIE*], **1993**(1), 86–97, SPIE (1993).

[4] Zhang, W. W., "Manufacture of mirror glass substrates for the nustar mission," in [*Proc. SPIE*], **7437**(1), 74370N–74370N–11, SPIE (2009).

[5] Goodwin, E. P., [*Field Guide to Interferometric Optical Testing*], vol. v. FG10, SPIE, Wageningen (2006).

[6] Bloemhof, E. E., "Absolute surface metrology by differencing spatially shifted maps from a phase-shifting interferometer," *Opt. Lett.* **35**, 2346–2348 (Jul 2010).

[7] Griesmann, U., "Three-flat test solutions based on simple mirror symmetry," *Appl. Opt.* **45**(23), 5856–5865 (2006).

[8] Huang, Y., Ma, J., Yuan, C., Pruss, C., Sun, W., Liu, M., Zhu, R., Gao, Z., and Osten, W., "Absolute test for cylindrical surfaces using the conjugate differential method," *Opt. Eng.* **55**(11), 114104–114104 (2016).

[9] VanSpeybroeck, L. P. and Chase, R. C., "Design parameters of paraboloid-hyperboloid telescopes for x-ray astronomy," *Appl. Opt.* **11**, 440–445 (Feb 1972).

[10] Shipley, A. F., Cash, W. C., Gendreau, K. C., and Gallagher, D. J., "Maxim interferometer tolerances and tradeoffs," in [*Proc. SPIE*], **4851**(1), 568–577, SPIE (2003).

[11] Chalifoux, B. D., Heilmann, R. K., Marshall, H. L., and Schattenburg, M. L., "Optical design of diffraction-limited x-ray telescopes," *Appl. Opt.* **59**(16), 4901–4914 (2020).

[12] Uttley, P., Hartog, R. d., Bambi, C., Barret, D., Bianchi, S., Bursa, M., Cappi, M., Casella, P., Cash, W., Costantini, E., Dauser, T., Diaz Trigo, M., Geneau, K., Grinberg, V., Herder, J.-W. d., Ingram, A., Kara, E., Markoff, S., Mingo, B., Panessa, F., Poppenhäger, K., RóŻańska, A., Svoboda, J., Wijers, R., Willingale, R., Wilms, J., and Wise, M., "The high energy universe at ultra-high resolution: the power and promise of x-ray interferometry," *Exp. Astron.* **51**(3), 1081–1107 (2021).

[13] Podgorski, W. A., Bookbinder, J., Content, D. A., Davis, W. N., Freeman, M. D., Hair, J. H., Owens, S. M., Petre, R., Reid, P., Saha, T. T., Stewart, J. W., and Zhang, W. W., "Constellation-x spectroscopy x-ray telescope optical assembly pathfinder image error budget and performance prediction," in [*Proc. SPIE*], **5168**, 318–333, SPIE (2003).

[14] Gao, W., Yokoyama, J., Kojima, H., and Kiyono, S., "Precision measurement of cylinder straightness using a scanning multi-probe system," *Precis. Eng.* **26**(3), 279–288 (2002).

[15] Elster, C., Weingärtner, I., and Schulz, M., "Coupled distance sensor systems for high-accuracy topography measurement: Accounting for scanning stage and systematic sensor errors," *Precis. Eng.* **30**(1), 32–38 (2006).

[16] Bloemhof, E. E., "Absolute surface metrology with a phase-shifting interferometer for incommensurate transverse spatial shifts," *Appl. Opt.* **53**, 792–797 (Feb 2014).

[17] Wisniewski, H. J., Whalen, M. M., Heilmann, R. K., Schattenburg, M. L., and Chalifoux, B. D., "Lateral shift mapping metrology for x-ray telescope mirrors," **11822**, 118220X–118220X–11, SPIE (2021).

[18] Wisniewski, H. J., Arnold, I. J., Heilmann, R. K., Schattenburg, M. L., and Chalifoux, B. D., "Axial shift mapping metrology for x-ray telescope mirrors," **12181**, 121814X–121814X–9, SPIE (2022).

[19] Penrose, R., "A generalized inverse for matrices," *Mathematical Proceedings of the Cambridge Philosophical Society* **51**(3), 406–413 (1955).

[20] Huang, L., Wang, T., Nicolas, J., Vivo, A., Polack, F., Thomasset, M., Zuo, C., Tayabaly, K., Wook Kim, D., and Idir, M., "Two-dimensional stitching interferometry for self-calibration of high-order additive systematic errors," *Opt. Express* **27**(19), 26940–26956 (2019).

[21] Robinson, B. M. and Reardon, P. J., "First-order perturbations of reflective surfaces and their effects in interferometric testing of mirrors," *J. Mod. Opt.* **52**(18), 2625–2636 (2005).

[22] Salsbury, C., *Spectrally Controlled Interferometry: Methods and Applications*, PhD thesis, The University of Arizona. (2018).